JOURNAL OF THE MECHANICAL BEHAVIOR OF BIOMEDICAL MATERIALS 31 (2014) 45–54

Available online at www.sciencedirect.com

ScienceDirect

www.elsevier.com/locate/jmbbm

Research paper

Innovative tribometer for *in situ* spectroscopic analyses of wear mechanisms and phase transformation in ceramic femoral heads

Leonardo Puppulin[a,*], *Andrea Leto*[b], *Zhu Wenliang*[c], *Nobuhiko Sugano*[c], *Giuseppe Pezzotti*[a,d]

[a]*Ceramic Physics Laboratory & Research Institute for Nanoscience, Kyoto Institute of Technology, Sakyo-ku, Matsugasaki, 606-8585 Kyoto, Japan*
[b]*Piezotech Japan, Ltd., Mukaibata-cho, Ichijoji, 606-8326 Kyoto, Japan*
[c]*Department of Medical Engineering for Treatment of Bone and Joint Disorders, Osaka University, 2-2 Yamadaoka, Suita, Osaka 565-0854, Japan*
[d]*The Center for Advanced Medical Engineering and Informatics, Osaka University, 2-2 Yamadaoka, Suita, Osaka 565-0871, Japan*

ARTICLE INFO

Article history:
Received 30 July 2012
Received in revised form
21 December 2012
Accepted 8 January 2013
Available online 23 January 2013

ABSTRACT

The literature on tribological assessments of artificial hip joints usually focuses on correlations between joint composition, size, and specific wear rates, but conspicuously ignores the physical aspects behind the occurrence of degradation mechanisms of friction and wear. Surface degradation in artificial joints occurs because of increases in temperature and local exacerbation of contact stresses inside the moving contact as a consequence of physical and chemical modifications of the sliding surfaces. This article reports about the development of a new pin-on-ball spectroscopy-assisted tribometer device that enables investigating also physical rather than merely engineering aspects of wear processes using *in situ* Raman and fluorescence techniques. This innovative tribometer is designed to bring about, in addition to conventional tribological parameters, also information of temperature, stress and phase transformations in the femoral heads as received from the manufacturer. Raman and fluorescence spectra at the point of sliding contact are recorded durilng reciprocating hard-on-hard dry-sliding tests. Preliminary results were collected on two different commercially available ceramic-on-ceramic hip joint bearing couples, made of monolithic alumina and alumina–zirconia composites. Although the composite couple showed direct evidence of tetragonal-to-monoclinic phase transformation, which enhanced the coefficient of friction, the specific wear rate was significantly lower than that of the monolithic one (i.e., by a factor 2.63 and 4.48 on the pin and head side, respectively). *In situ* collected data compared to *ex situ* analyses elucidated the surface degradation processes and clarified the origin for the higher wear resistance of the composite as compared to the monolithic couple.

*Corresponding author. Tel.: +81 0757 247 568.
E-mail address: puppulin@chem.kit.ac.jp (L. Puppulin).

1751-6161/$ - see front matter © 2013 Elsevier Ltd. All rights reserved.
http://dx.doi.org/10.1016/j.jmbbm.2013.01.004

1. Introduction

Tribological studies of ceramic-on-ceramic joint components are usually carried out using joint simulators (Saikko, 2005; Goldsmith and Dowson, 1999; McKellop and D'Lima, 2008). Such equipments provide phenomenological output parameters for describing the wear effect, namely, the friction coefficient, the material loss rate, and the roughness of the bearing surface upon topographic analyses at the end of wear testing (Nevelos et al., 2001; Scholes et al., 2004; Al-Hajjar et al., 2012), but they conspicuously ignore the physical circumstances leading to wear degradation. In an attempt to provide this missing information, our research group has recently published a series of papers (Pezzotti et al., 2006, 2007; Pezzotti, 2005, 2007; Pezzotti and Porporati, 2004; Puppulin et al., 2011), which demonstrate the efficacy of advanced spectroscopic Raman and fluorescence (microprobe) analyses in obtaining a deeper understanding of the microscopic mechanisms behind the wear behavior of bioceramic bearings, as they typically lie on the microscopic scale. A full elucidation of the physical, mechanical and chemical state of the worn surfaces, as obtained through advanced spectroscopic methods is believed to be particularly relevant for further improving the manufacturing process of ceramic-on-ceramic bearings, namely the most advanced protagonists in joint arthroplastic applications. Building upon the knowledge of different characterization methods, it seemed to us a quite natural evolution in joint surface metrology to combine tribological and spectroscopic assessments, in order to obtain an advanced and more comprehensive wear characterization method, which could provide not only conventional tribological parameters but also spectroscopic outputs.

Surface characterization using photo-stimulated spectroscopy at the contact during tribological tests (hereafter referred to as *in-situ* analysis) is actually not a new idea, several attempts having already been reported in the literature dealing with different fields of research (Singer et al., 2001; Joly-Pottuz et al., 2007, Cherif et al., 1997). In a recent review paper, Singer et al. (2001) gave a comprehensive discussion about a number of published investigations of third-body wear and friction of protective coatings in which the contacts were separated at the end of the sliding test before being analyzed (hereafter referred to as *ex situ* analysis). In that paper, *in situ* tribological studies were also newly described, which included concurrent analyses by optical microscopy and Raman spectroscopy. *In situ* analyses provided additional (and yet missing) evidences that directly correlated third body processes to friction and wear behavior of different low-friction coatings. Joly-Pottuz et al. (2007) performed *in situ* experiments to study modifications of nanoparticles as lubricant additives (*e.g.*, inorganic fullerenes and carbon nanotubes). Information on lubrication mechanisms and real-time structural changes of nanoparticles inside the contact area could be obtained, which newly revealed tribologically active behaviors, progressive exfoliation and amorphization processes. Both the above-mentioned analyses were quite successful in bringing new physical insight into the studied tribological phenomena. However, there was a common denominator in the experimental setup adopted in the above investigations: in the pin-on-disk configuration of the *in situ* tribometer placed under the microscope for spectrophotometer analyses, one of the sliding counterparts was made of a transparent material (e.g., glass or sapphire) in order to allow focusing the laser on the contact counter-surface. In other words, for the selected *in situ* tribometer configuration, the choice of at least one of the components of the sliding couple was mandatorily constrained by laser transparency issues. Cherif et al. (1997) used a different approach to investigate *in situ* wear processes in alumina-zirconia composite. Those researchers measured the temperature in the mid-thickness of the disk during tribological tests using a thermocouple fixed by alumina cement in a hole drilled in the worn disk. In their experimental set-up, however, serious issues arose, related to measurement accuracy. Since the temperature field in a ceramic component decades rather quickly in space away from the contact point, the measured temperature was far from representing the real contact temperature of the sliding surfaces. In summary, the so far presented outputs of *in situ* tribometry approaches (Singer et al., 2001; Joly-Pottuz et al., 2007, Cherif et al., 1997) have been either lacking of accuracy or resulted severely narrowed in their significance by the constrained choice of at least one "artificial" sliding component.

Keeping in mind the basic notions mentioned above and being aware that tribological characterizations of hip joints should not be hindered by the above limitations, we have attempted developing a new tribometer device that could enable concurrent tribological and spectroscopic characterizations *in situ* at the contact point of sliding wear with high accuracy and without altering the nature of the sliding counterparts. Besides conventional tribological outputs, this new *in situ* device is shown capable to monitor phase transformation fractions, local contact stress and temperature, as these parameters develop at the contact point with increasing sliding distance. A detailed description of this advanced device is reported for the first time in this paper together with some preliminary results collected on two different types of commercially available ceramic-on-ceramic hip joint bearing couples.

2. Experimental procedures

2.1. *Photo-stimulated spectroscopy-assisted tribometer device*

A detailed description is given hereafter of the new instrument designed to concurrently perform tribological tests on ceramic femoral heads and collect Raman or fluorescence spectra by means of an *in situ* confocal spectrophotometer. The tribometer, schematically shown in Fig. 1(a), consists of several component parts (labeled (aa)–(hh) in Fig. 1(a)). The selected sliding configuration foresees a rotating and a fix element (*i.e.*, henceforth referred to as the femoral head ball and the pin, respectively). A stainless steel taper (aa), 74 mm in length, was used to tightly grip the ceramic femoral head (bb) to its rotating axis. The taper (conical) head profile was of an interchangeable type and could be specifically shaped to

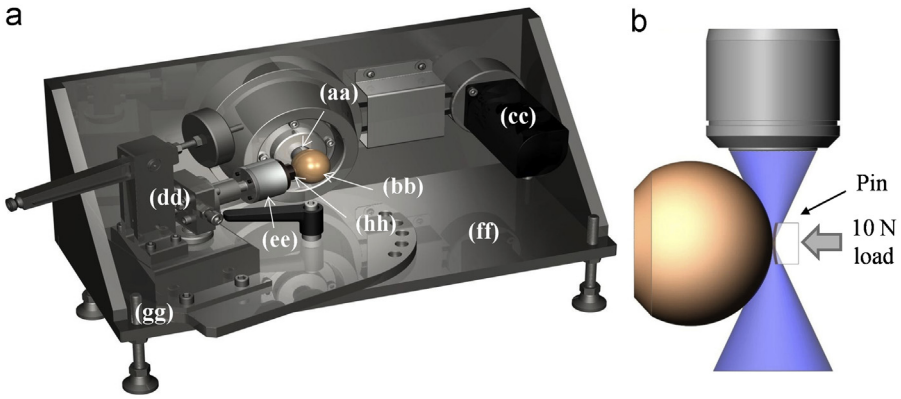

Fig. 1 – (a) Schematics of the tribometer (a) and of the interaction between laser beam and sliding couple (b). In (a), the function of each component part (labeled (aa)–(hh) is explained in the text.

match the different standard tapers adopted by the femoral head maker. A driver system (cc), which rotated the femoral head, was attached to an AC electrical servomotor, namely an engine capable of giving a controllable sliding speed that was stable under the influence of the frictional forces generated during testing. The angular velocity could be varied either in continuous or in step mode. The 'step mode' provided a useful way to keep the sliding speed constant (e.g., equal to 0.1 m/s, in the case of the present experiments), while using different ball/pin contact angles. The contact angle, namely the angle between the axis of the rotating ball (i.e., head) and that of the non-rotating pin, could be adjusted in the angular interval 0°–60°. Motor and belt transmission were selected to minimize the vibrations transmitted to the femoral head and to keep the fluctuations of the contact point between ball and pin in the radial range of $<\pm 5\,\mu m$. The loading mechanism (dd) was designed to apply a controlled load to the pin holder through a lever-arm device attached to a dead-weight loading system. Such a mechanism could be rotated with respect to its vertical axis to vary, as already mentioned, the ball/pin contact angle. The load pushing the pin against the femoral head could be applied in three different magnitudes, namely 10, 20, and 30 N. A biaxial load cell (ee) was used, which was capable to concurrently measure the actual axial force, F_z, and the frictional force, F_x, (i.e., the forces perpendicular and parallel to the head surface) developed during sliding on the femoral head within a range of 0–50 N. The selected load cell possessed excellent thermal stability ($\pm$0.05% R.O./°C), good load/volt linear response (<2%) and low hysteresis ($\pm$0.1% R.O.). The load cell also allowed for off-centering the applied load (X–Y: $\pm$2.5 mm and Z: $\pm$5 mm) without significantly altering the measurement outputs. The tribometer stage (ff) had the only function of firmly fitting the tribometer equipment onto the X–Y–Z stage of the spectrometer device. As a tool for obtaining independent positioning on the spectrometer stage, the tribometer stage was equipped with three adjustable studs (gg), which served to regulate height in an interval of $\pm 10\,\mu m$, as well as the tribometer inclination in the interval 0°–10°. In the control panel, the operator could set recording of rotating speed, sliding distance, and F_z and F_x values. Because of the rapid fluctuation of the involved forces, the tribometer controller needed to be connected to a data logger that sampled and stored the mechanical outputs. The pin (hh) was a $5 \times 5\,mm^2$ section cut obtained from the dome of a separate femoral head made of the same material of the tested one. The peculiar design of the tribometer was specifically conceived to focus the laser on the contact point between the pin and the femoral head, and to collect the backscattered signal during the tribological test, as shown in Fig. 1(b). Schematics of the head and of the pin used in the present experiments are shown in Fig. 2(a) and (b), respectively. Note that, in the adopted experimental setup, both pin and head rigorously keep the sphericity and all the other surface characteristics of the original hip implant, so that the wear phenomenon occurs on real components rather than on model materials. Nevertheless, we deal here with a (more severe) convex-convex surface configuration as compared to convex-concave one. Moreover, in a real joint, there is a continuous variation of the contact point due to joint clearance, while in the present test sliding occurs rigorously along the same geometrical trajectory.

It is a general issue that all tribological tests performed in laboratory conditions, especially those aimed at clarifying the intrinsic wear properties of the sliding couple (e.g., pin-on-disk testing), operate under conditions that might greatly differ from the conditions experienced by bearings during clinical use. However, in the present testing procedure, a series of geometrical and mechanical parameters including sliding speed, ball/pin contact angle, and the magnitude of the applied load could be adjusted for compensating the effect of different curvatures in order to match international standards for wear testing, as better explained in the next section. Moreover, operating under conservative (i.e., more severe) conditions as compared to *in vivo* tribological conditions represents a correct testing approach. In support to this latter point, we notice that one generally assumes the contact between the sliding counterfaces *in vivo* to be mediated through a fluid film (i.e., a particularly relevant feature for ceramic-on-ceramic bearings with high wettability). However, ceramic-on-ceramic hip joints have also been reported in several cases to actually operate in 'dry-joint' conditions (DelaValle and McCook, 2008; Chevillotte et al., 2010; Currier et al., 2010). This is a consequence of the fluid film thickness decreasing or being interrupted, with the ceramic components coming into contact essentially unlubricated. From this viewpoint, one might regard to be appropriate setting the

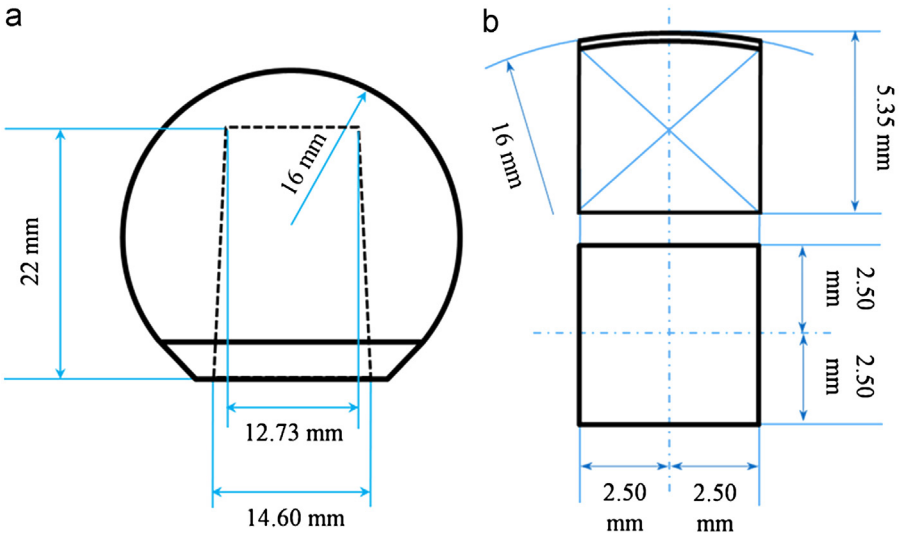

Fig. 2 – Schematics with the dimensions of the head (a) and of the pin (b) used in the present wear experiments.

conditions for *in vitro* wear testing to a necessarily higher degree of severity as compared to ideal conditions *in vivo*.

2.2. *Wear testing procedures*

Before testing the femoral head and the pin were washed ultrasonically in high purity acetone for 0.5 h, and then immediately rinsed with high purity ethanol and dried for additional 0.5 h at room temperature. Prior to clamping the sliding parts to their respective holders, their weight was accurately measured. After mounting both pin and femoral head in the tribometer machine, the eccentricity of the rotating ball was checked using a profilometer and adjusted using a bolt to $<10\,\mu m$. The pin and the attached weight system were then rotated to form the desired contact angle between pin and ball head (i.e., 45° in this study). The tribometer device was finally allocated inside the spectrometer equipment, and the incoming laser beam focused through a long-focus objective lens at the contact point between pin and ball, as better explained in the following section. Throughout all wear tests described in this study a load of 10 N was applied to the pin in contact with the ball and the sliding velocity of 0.1 m/s was set on the tribometer controller. The tests were always divided into two steps: (i) a pre-testing step lasting about 30 min, in which sample positioning and various other adjustments were performed in order to allow all test parameters reaching stability; and, (ii) the main tribological test that lasted for about 6 h and was terminated when the sliding distance reached the value of 2×10^3 m. All wear tests were on self-mating couples and were carried out at room temperature under dry sliding conditions. The dynamical conditions selected in the present pin-on-ball wear testing configuration were fixed in order to obtain a precise correspondence with the recommendations given by international standard for the pin-on-disk wear testing configuration (i.e., ASTM G99/G95, DIN 50324 and ISO/FDIS 20808:2003(E)).

2.3. *Spectroscopic procedures*

The design of the new tribometer was specifically conceived to enable focusing the laser beam at the contact point between pin and femoral head, and to collect *in situ* the backscattered Raman or fluorescence signals during the tribological test. The interaction between laser beam and sliding couple is schematically shown in Fig. 1(b). Raman spectra were collected with a triple monochromator spectrometer (T-64000, ISA Jobin-Ivon/Horiba Group, Tokyo, Japan) equipped with a charge-coupled detector (high-resolution CCD camera). The laser excitation source was the monochromatic blue line emitted by an Ar-ion laser at a wavelength of 488 nm and the power on the surface was set at 400 mW. The spectral integration time was typically 60 s for collecting zirconia and alumina Raman spectra, while 1 s sufficed for collecting the fluorescence signal emitted from substitutional Cr^{3+} elements contained in the alumina lattice. All the spectroscopic experiments were conducted with focusing the waist of the laser beam on the material through an optical lens. Raman and fluorescence backscattered light was then re-focused onto a pinhole and transmitted into the spectrometer via the same optical lens used to focus the incoming laser. Backscattered light dispersion onto a CCD camera finally allowed displaying Raman or luminescence spectra. The spatial resolution of the measurements was greatly affected by the cross slit (pinhole) aperture. Reducing the pinhole diameter enabled cutting the light scattered from substantial portions of the probed volume above and below the selected focal plane. The highest spatial resolution (in the order of few microns) that could be obtained corresponded to a cross-slit diameter of 100 μm. Such aperture diameter was found to represent a threshold value. Increasing the pinhole diameter above this threshold increased the intensity of the collected signal, thus reducing the integration time needed for collecting a Raman spectrum of good quality, but also involved significantly larger probe volumes. On the other hand, further reducing the pinhole diameter led to unacceptably low efficiencies, and thus far too long spectral integration times, for collecting clear signal intensities.

Monoclinic zirconia volume fractions, V_m, were quantitatively evaluated from the relative intensities of selected Raman bands belonging to the tetragonal (145 cm^{-1}) and to the monoclinic (178 cm^{-1} and 189 cm^{-1}) polymorphs. The following equation was used, according to Katagiri et al. (1988):

$$V_m = \frac{0.5(I^{(m)}_{189} + I^{(m)}_{178})}{0.5(I^{(m)}_{189} + I^{(m)}_{178}) + 2.2I^{(t)}_{145}} \quad (1)$$

where I is the intensity of a Raman band belonging to the polymorph indicated by the superscript in brackets ((*m*) and (*t*) for monoclinic and tetragonal polymorph, respectively) and spectrally located at the frequency given in the subscript.

Residual stress assessments on the surface of the worn samples after the end of the tribological test were made by means of a piezo-spectroscopic approach on the frequency shift of the chromophoric fluorescence bands emitted from the alumina phase (Ma and Clarke, 1994). The temperature increase at the contact point of the sliding couple was determined from the increase of the full width at half maximum of the chromophoric fluorescence emitted by substitutional Cr^{3+} elements in the Al_2O_3 lattice (McCumber and Sturge, 1963). The latter assessment required a deconvolution procedure to be applied to the raw experimental data in order to eliminate the effect of the finite size of the fluorescence probe. Such procedure is computationally complex and requires preliminary calibrations of the interaction between the laser probe and the sliding couples. The full computational details, the calibrations, and the algorithms enabling stress and temperature measurements from fluorescence spectra are described in a companion paper (Zhu et al., in press).

2.4. Specific wear rate and coefficients of friction

At the end of the wear test, both femoral head and pin samples were ultrasonically cleaned to remove ceramic and metal debris formed at the taper joint. Then, the weights of the worn pin and ball were measured and subtracted from the respective pristine weights before wear test. In addition, the worn surfaces were observed by optical microscopy in order to visualize the elliptical scar on the pin and the longitudinal scar on the femoral head as created during the dry-sliding process. Optical inspections served for the quantitative evaluation of the length of the elliptical axes of the pin scar and of the average width of the longitudinal scar on the femoral head. These geometrical parameters were necessary for quantifying the average volume loss and calculate the specific wear rates. The worn-out volumes of the pin, V_p, and of the femoral head, V_h, are given by following equations:

$$V_p = \frac{\pi a^3 b}{64R} \quad (2)$$

$$V_h = 2\pi r S \quad (3)$$

where a and b are the lengths of the short and long axes of the elliptical pin scar, respectively; R is the radius of curvature of the pin; r is the radius of the trajectory of the wear scar on the head sample, and S is its average cross sectional area. Note that Eq. (2) can only be used in the case of $b < 1.5a$, otherwise the wear volume must be calculated by accurately profiling the wear scar with a profilometer. The difficulty in detecting a reliable value of the scar depth in the femoral head due to the high wear resistance of the two materials led us to assess the volume loss by measuring the mass loss and dividing it by the density of the material. The specific wear rates for the pin, W_p, and for the head, W_h, could then be computed according to the respectively measured worn volumes, as follows:

$$W_{p(h)} = \frac{V_{p(h)}}{FL} \quad (4)$$

where F is the applied force (i.e., 10 N) and L is the sliding distance in the wear test.

The coefficient of friction, μ, a function of sliding distance, could be calculated as the ratio of the measured frictional force to the axial force component. In the characterizations described in this paper, we will present both the coefficient of friction in the transient period of initial sliding and its value as successively reached at the steady state of the wear process.

2.5. Investigated materials

The investigated sliding couples were obtained from two kinds of commercially available ceramic biomaterials employed in artificial hip joints: BIOLOX®*delta* and BIOLOX®*forte* (both manufactured by CeramTec, Plochingen, Germany). BIOLOX®*delta* is a composite material, which consisted of 80 vol% Al_2O_3, 17 vol% ZrO_2, and 3 vol% strontium aluminate. Y_2O_3, and Cr_2O_3 were added to the raw materials in quantities of 0.6 and 0.3 wt%, respectively, in addition to a small amount of SrO. After sintering, Y and Cr elements were mainly solved in the grain structure. No porosity could be observed in the microstructural arrangement, and the sizes of alumina and zirconia grains were 1.0 and 0.3 μm, respectively. The BIOLOX®*forte* material was made of monolithic (high-purity) polycrystalline alumina. The average size of the alumina grains was 1.4 μm. Composite and monolithic self-mating biomaterials are henceforth simply referred to as *delta*-on-*delta* and *forte*-on-*forte* sliding couples, respectively. All the analyzed femoral heads were 32 mm in diameter, and were self-worn against pins with the same surface curvature of the femoral head.

The surface of the samples before and after wear tests were observed by field-emission-gun scanning electron microscope (FEG-SEM, SE-4300, Hitachi Co., Tokyo, Japan) in order to provide the microstructural details of the wear damages.

3. Results and discussion

3.1. Wear testing results

The outputs of wear tests on the two different self-mating ceramic-on-ceramic couples, namely the monolithic *forte*-on-*forte* and the composite *delta*-on-*delta* couples, are summarized and compared in this section. Fig. 3(a) and (b) shows optical micrographs of the damaged zone and the related width measurements on the ball side for the *forte*-on-*forte*

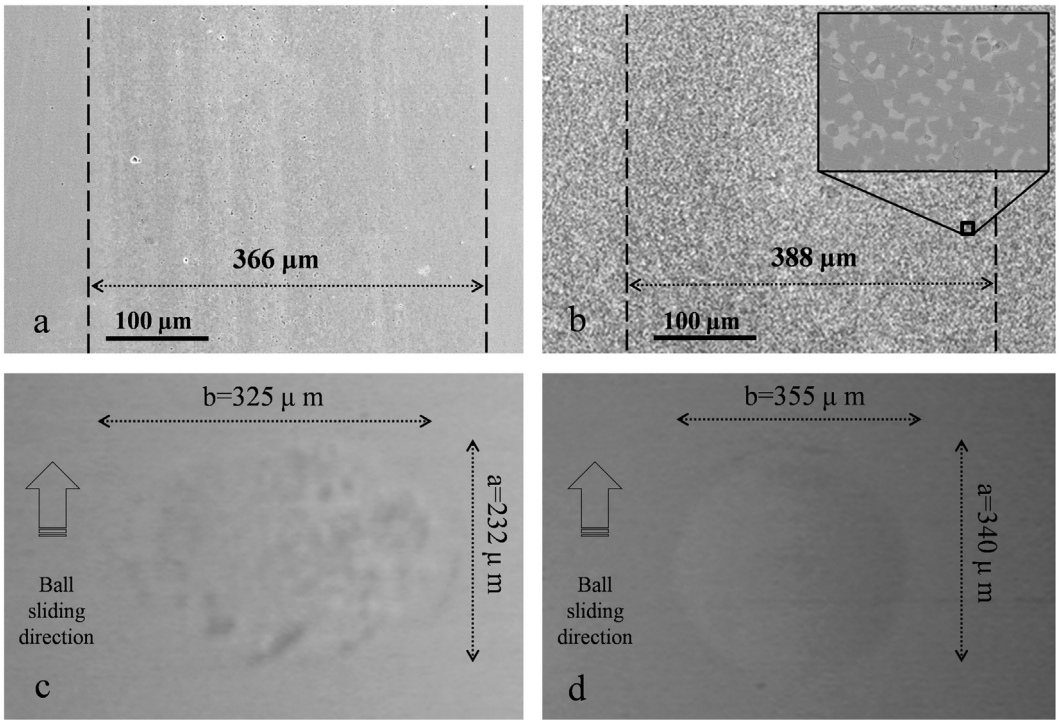

Fig. 3 – In (a) and (b), optical micrographs of the damaged zone and related length measurements on the head side for the *forte*-on-*forte* and *delta*-on-*delta* couple, respectively, as observed at the end of the respective wear tests conducted for a sliding distance of 2×10^3 m. Wear damage in *delta*-on-*delta* femoral head was detectable only at higher magnification, as shown in the inset of (b). In (c) and (d), micrographs of wear scars, as observed after wear tests on the pin side for the monolithic and the composite couples, respectively.

Table 1 – Tribological results of the wear tests.

	Biolox®*forte*	Biolox®*delta*
Scar width (pin side) [µm]	325	355
Scar width (ball side) [µm]	366	388
Specific wear rate (pin) [mm^3/Nm]	9.671×10^{-9}	3.67×10^{-9}
Specific wear rate (ball) [mm^3/Nm]	1×10^{-10}	2.23×10^{-11}
Coefficient of friction (initial)	0.38	0.43
Coefficient of friction (regime)	0.41	0.52

and *delta*-on-*delta* couple, respectively, as observed at the end of the respective wear tests using the same magnification (250 ×). While for the *forte*-on-*forte* the location of the scar was easily detectable, in the case of *delta*-on-*delta* the scar width measurement required a higher magnification to identify the worn surface, as shown in the inset of Fig. 3(b). In the same Fig. 3, optical micrographs of the elliptical wear scars, as observed after wear tests on the pin side, are shown for the monolithic and the composite couples (in (c) and (d), respectively). According to the width measurements done on the optical micrographs (summarized in Table 1) and the mass loss, the specific wear rates on pin and ball could be calculated and the results are listed in Table 1. Interestingly, the composite couple showed slightly wider but significantly lower specific wear rate, namely a shallower scar damages on ball side as compared to the monolithic one. The extreme shallowness of the scar even under such a severe test condition made the detection of its depth quite difficult to perform with a conventional stylus profilometer, thus proving the extremely high wear resistance of the composite. The elliptical scar on the pin was also shallower than the monolithic one and closer to a circular morphology. Accordingly, the specific wear rate of the composite couple was about 2.63 and 4.48 times lower than the monolithic one on the pin and the head side, respectively. The friction coefficients were also distinctly different between the two investigated couples (cf. Table 1), consistently showing values higher by about 12% and 20% in the *delta*-on-*delta* couple for initial and regime conditions, respectively. This difference can be ascribed to the intrinsically higher friction coefficient of zirconia as compared to alumina. Our results are consistent to that of Kerkwijk et al. (1999), which investigated the friction and wear response wear response in alumina and zirconia toughened alumina (ZTA) using a classic pin-on-disc tribometer.

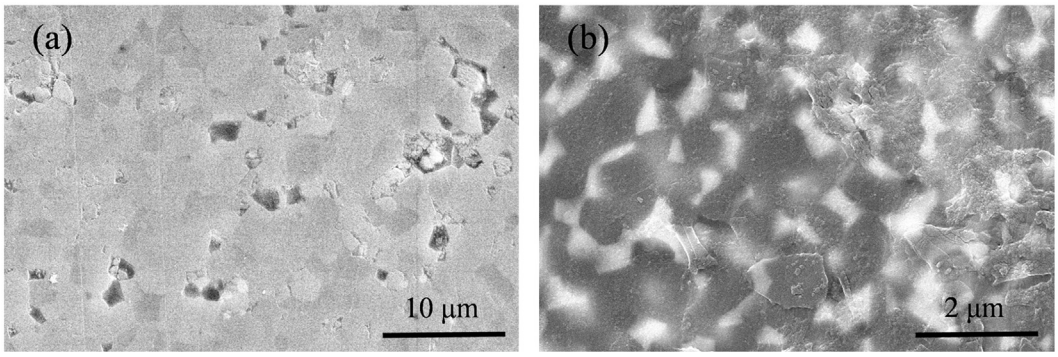

Fig. 4 – In (a) and (b), FEG-SEM micrographs taken in the damage scar region of the *forte*-on-*forte* and *delta*-on-*delta* couple, respectively.

Fig. 4(a) and (b) show FEG-SEM micrographs taken in the damaged scar regions of the *forte*-on-*forte* and *delta*-on-*delta* couple, respectively. The micrographs reveal a quite high level of surface damage in the monolithic couple, with significant grain detachment. On the other hand, the damage on the surface of the composite material was limited to micro-scratches and partial detachments, while only sporadically zirconia grains were pulled out from the worn surface (none is indeed seen in the shown micrograph). In summarizing the comparison of the tribological characteristics of the tested monolithic and composite hard-on-hard couples, it could be said that, despite a larger friction coefficient and the apparently wider (but quite shallow) damage scar measured on the head of the composite couple, this couple was by far more resistant to grain detachment and wore at a significantly lower rate as compared to the monolithic couple. As discussed in a previous paper (Pezzotti et al., 2010), there are two distinct reasons for the enhanced wear resistance of the alumina matrix of the composite material and monolithic alumina, of chemical and mechanical nature, respectively. On the chemical side, it is the addition of Cr-dopant in the composite (absent in the monolithic) material that is responsible for a surface configuration at the molecular scale less prone to oxygen vacancy formation. On the mechanical side, a strongly compressive residual stress was found stored in the Al_2O_3 matrix phase at the surface of the composite component, which was not found in the monolithic one. Such high residual stress magnitude was partly due to a thermal expansion mismatch between the constituent alumina and zirconia phases and partly related to the surface chemistry conditions, as described above.

3.2. *In situ and ex situ Raman and fluorescence spectroscopy*

Fig. 5(a) shows a typical confocal Raman spectrum collected *in situ* from the contact point of the sliding composite couple. In the spectrum, tetragonal and monoclinic bands are labeled and, from their intensities, the volume fraction of monoclinic phase, V_m, could be calculated according to Eq. (1). Similar spectra were collected as a function of sliding distance, L, thus obtaining a plot of $V_m(L)$, as shown in Fig. 5(b). Plots are given for two different configurations of the Raman probe, namely a confocal configuration (*i.e.*, 100 μm pinhole aperture) and a configuration with the full aperture of the confocal pinhole (referred to as "through focus" in the label). The two different optical configurations lead to different laser penetration depths in Raman assessments, in the order of few microns and few tens of microns for the cases of confocal and through-focus assessments, respectively. The plot collected with a confocal probe indeed shows a clear increase (in the order of 35%) of monoclinic content after $L=2\times10^3$ m, above the initial content of monoclinic polymorph, $V_m^{(0)}\approx15\%$, in the pristine material. The values recorded by the through-focus configuration are conspicuously lower, showing a monoclinic volume fraction increase from about 5% in the pristine composite to 7.5% at the end of the test (i.e., increase also in the order of 33%). The locally occurred polymorphic transformation is obviously a consequence of the stress and temperature increases at the contact point during dry sliding. However, the extent of transformation along the depth of the sample appears confined to a shallow region, because, unlike the confocal probe, the through-focus probe conspicuously fails in locating any amount of monoclinic fraction on the sample surface. The temperature increase measured *in situ* (i.e., concurrently to polymorphic transformation) from the linewidth of the chromophoric emission of alumina was found to be in the order of 134 °C (vs. 48 °C in the monolithic couple) and to decade very quickly (i.e., within about 2 μm) with distance from the contact point (Zhu et al., in press). Since the polymorphic transformation occurs with substantial volume increase, it can be one additional reason for the higher coefficient of friction measured in the composite couple (cf. Table 1). The plot in Fig. 5(b) should be compared to a plot of monoclinic fraction across the scar on the ball head, as performed *ex situ* after the end of the tribological test on the worn sample. This plot is given in Fig. 6(a) for both confocal and through-focus probe configurations. The two different probe configurations again show different values when recorded at the same locations due to the different probe depths, but the values of monoclinic phase found *ex situ* for both confocal and through-focus plots at the center of the scar were very close to those measured *in-situ* during tribological tests. An intriguing finding was that a relatively high content (up to about 32%) of monoclinic phase was found at a distance of about 300 μm from the center of the scar, namely quite far from the distance of the developed gradient of temperature. The lower value measured at the

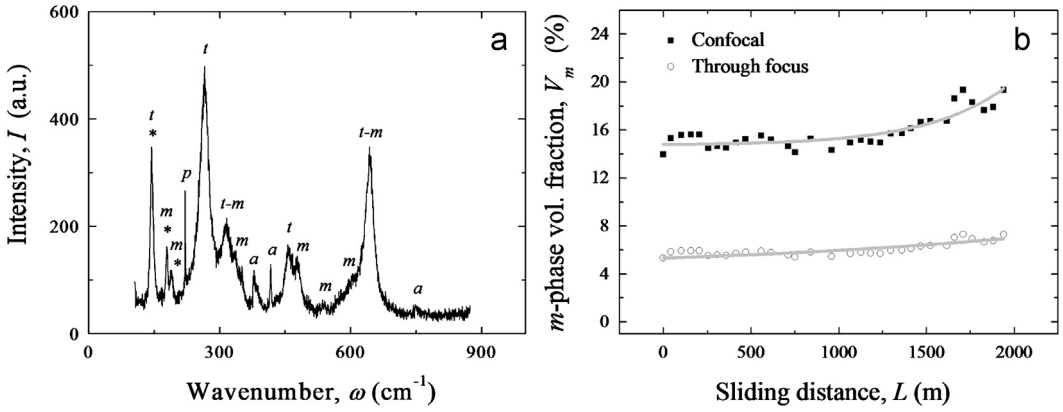

Fig. 5 – Typical Raman spectrum collected *in situ* from the contact point of the sliding composite couple. In the spectrum, tetragonal and monoclinic bands are labeled *t* and *m*, respectively (overlapping bands show both labels). The bands labeled with an asterisk were used for the computation of the monoclinic volume fraction. The label (a) refers to alumina bands, while the label *p* locates a selected plasma line from the laser emission, which was used as an internal standard for spectroscopic calibrations. (b) A plot of monoclinic volume fraction, V_m, is given as a function of sliding distance.

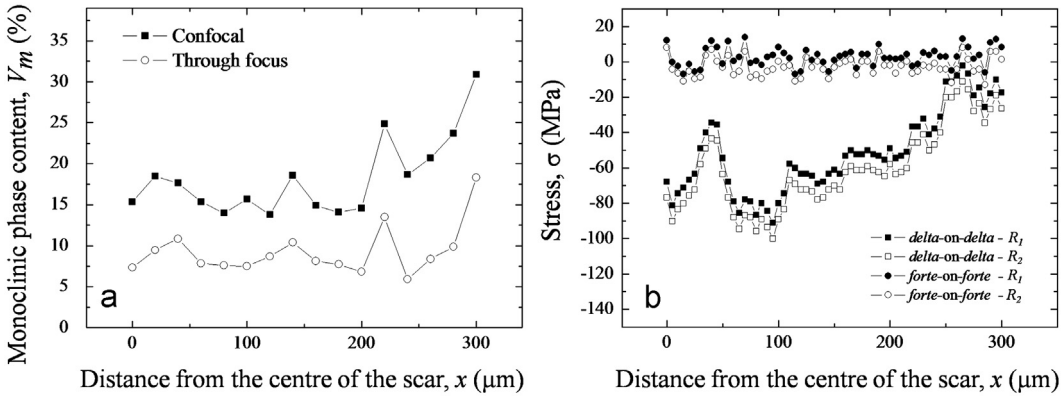

Fig. 6 – (a) Plot of monoclinic fraction across the scar on the ball head, as performed *ex situ* after the end of the tribological test on the worn sample. (b) *Ex situ* measured residual stresses are plotted as measured by collecting the fluorescence spectral shifts of the chromophoric doublet of the alumina phase in the worn monolithic and composite heads.

center of the scar cannot either be explained as being simply due to pullout of zirconia grains during tribological test, because we have found the occurrence of such phenomenon to be only sporadic in the present test. The agreement between *in situ* and *ex situ* monoclinic volume fraction measurements at the center of the scar also confirms that negligible further transformation occurred during cooling from the sliding regime temperature after the interruption of the tribological test. Therefore, the spatial gradient in monoclinic phase transformation found on the head scar should rather be attributed to the high stress gradients developed on the material surface during sliding than to temperature effects. From a general viewpoint, the trend found for monoclinic phase transformation during tribological test on the *delta*-on-*delta* couple could be interpreted as indicating high stability for the tetragonal zirconia dispersed in the alumina matrix of the composite. However, for ceramics used in joint arthroplasty, the *in vivo* performance of load-bearing surfaces depends on the combined effects of both structural and environmental loading. In the dry-sliding results presented in this paper, the effect induced by the exposure to biological environment is missing. Therefore, additional studies are needed with running the tribometer under wet conditions, namely in an environment that could reproduce as close as possible the real operative conditions encountered by the femoral head in the human body.

In Fig. 6(b), *ex situ* residual stresses were measured by collecting fluorescence spectra from the alumina phase along a line scan perpendicular to the scar, starting from the center of the worn area to a location 300 μm away from it. Spectral shifts, which represent the local differences in peak position with respect to the peak average position recorded before wear testing, were translated into hydrostatic stress magnitudes by means of the piezo-spectroscopic coefficients published by Ma and Clarke (1994). The region investigated was the same as in the case of the scan shown in Fig. 6(a). Two distinct fluorescence bands, due to Cr^{3+} impurities in Al_2O_3 (henceforth referred as *R*1 and *R*2 lines) (Ma and Clarke, 1994), provided consistent results, which showed a shift towards compressive values (*i.e.*, with respect to the unworn material) in a region near the center of the scar (abscissa $0 \leq x \leq 100$ μm), and a subsequent gradual stress release starting from $x = 100$ μm to 300 μm. The observed residual stress field in the

alumina phase belonging to the wear zone can be interpreted as the superposition of two components: one component of compressive nature arising from the hard-on-hard pressure contact during sliding (Deeg, 1992), and another component of tensile nature induced by the volume expansion associated with the polymorphic transformation of the zirconia phase (Sergo, 2004, Pezzotti et al., 2008). The effects of these two stress components are thus competitive with respect to the cumulative spectral shift recorded. Moreover, the high compressive stress component developed at the center of the scar seems to induce a delaying effect on tetragonal-to-monoclinic phase transformation. The results of *ex situ* experiments shown in Fig. 6(a) have indeed shown that polymorphic transformation preponderantly takes place at distances relatively far from the contact point, namely in regions at which the contact compressive stress is significantly released. A similar characterization of *ex situ* residual stresses in the monolithic alumina *forte*-on-*forte* couple (also shown for comparison in Fig. 6(b)) revealed stresses of negligible magnitude, as a consequence of the occurrence of significant grain pullout and surface disruption, which released the compressive contact stress, in addition to the absence of a transforming phase.

4. Conclusion

Both *ex situ* and *in situ* techniques for the tribological analysis of artificial hip biomedical implants have been presented. The *in situ* characterizations were carried out in a newly developed tribometer device that not only enabled wear testing under standard wear conditions, but also the concurrent collection of Raman and fluorescence spectra at the contact point. The tribological behaviors of two hard-on-hard sliding couples, namely a monolithic and a composite ceramic couple, were characterized and compared. The main outcomes of these characterizations can be summarized as follows:

(i) The composite sliding couple was significantly more wear resistant than the monolithic one under dry sliding conditions (specific wear rate significantly lower by a factor 2.63 and 4.48 on the pin and head side, respectively). This result is important when considering that the testing conditions adopted here were quite severe as compared to *in vivo* sliding conditions.

(ii) Polymorphic phase transformation, up to about 30 vol% of the original ZrO_2 fraction, occurred *in situ* under conditions of dry sliding in the composite couple, and it was considered as one of the causes of the higher friction coefficient measured in the composite couple as compared to the monolithic one.

(iii) The monolithic couple, which experienced significantly deeper scars and grain pullout after testing as compared to the composite couple, wore at three- to four-fold higher specific wear rates.

(iv) The degree of damage observed in the monolithic couple was quite high after sliding for 2×10^3 m, with severe grain pullout and partial disruption of the material surface. Some pullout of the zirconia grain was also observed but only sporadically in the composite sample. Nevertheless, the overall damage on the surface was clearly less pronounced than that found on the surface of the monolithic femoral head.

Finally, it could be useful to state again the limit of the present tribological investigation, which might reside in a scarce predictivity of the actual joint lifetime *in vivo*, given the extreme conditions and severity of wear testing adopted in dry sliding.

REFERENCES

Al-Hajjar, M., Fisher, J., Tipper, J., Williams, S., Jennings, L., 2012. Wear of ceramic-on-ceramic bearings in THRs: effect of head size under steep cup inclination angle and microseparation and edge loading conditions. Journal of Bone and Joint Surgery, British Volume 94B (Suppl. XL1).

Cherif, K., Gueroult, B., Rigaud, M., 1997. Al_2O_3–ZrO_2 debris life cycle during wear: effects of the third body on wear and friction. Wear 208, 161–168.

Chevillotte, C., Trousdale, R.T., Chen, Q., Guyen, O., An, K.N., 2010. Hip squeaking: a biomechanical study of ceramic-on-ceramic bearing surfaces. Clinical Orthopaedics and Related Research 468, 345–350.

Currier, J.H., Anderson, D.E., Van Citters, D.W., 2010. A proposed mechanism for squeaking of ceramic-on-ceramic hips. Wear 269, 782–789.

Deeg, E.W., 1992. New algorithms for calculating Hertzian stresses, deformations, and contact zone parameters. AMP Journal of Technology 2, 14–24.

DelaValle, A.G., McCook, N., 2008. Squeaking in total hip replacement: a cause of concern. Orthopedics 31 (9). Available from URL: 〈http://www.healio.com/orthopedics/hip/journals/ortho/%7B43f6d26c-91a649cc-af52-7fd8a43d7703%7D/squeaking-in-total-hip-replacement-a-cause-for-concern〉.

Goldsmith, A.A., Dowson, D., 1999. A multi-station hip joint simulator study of the performance of 22 mm diameter zirconia-ultra-high molecular weight polyethylene total replacement hip joints. Proceedings of the Institution of Mechanical Engineers—Part H: Journal of Engineering in Medicine 213, 77–90.

Joly-Pottuz, L., Martin, J.M., Belin, M., Dassanoy, F., 2007. Sudy of inorganic fullerenes and carbon nanotubes by *in situ* Raman tribometry. Applied Physics Letters 91, 153107-1–153107-3.

Katagiri, G., Ishida, H., Ishitani, A., Masaki, T., 1988. Direct determination by Raman microprobe of the transformation zone size in Y_2O_3 containing tetragonal ZrO_2 polycrystals. In: Somiya, S., Yamamoto, N., Yanagida, H. (Eds.), Advances in Ceramics. Science and Technology of Zirconia III, vol. 24. The American Ceramic Society, Columbus, OH, pp. 537–544.

Kerkwijk, B., Winnubst, A.J.A., Verweij, H., Mulder, E.J., Metselaar, H.S.C., Schipper, D.J., 1999. Tribological properties of nanoscale alumina–zirconia composites. Wear 225–229, 1293–1302.

Ma, Q., Clarke, D.R., 1994. Piezospectroscopic determination of residual stresses in polycrystalline alumina. Journal of the American Ceramic Society 77, 298–302.

McCumber, D.E., Sturge, M.D., 1963. Linewidth and temperature shift of the R lines in ruby. Journal of Applied Physics 34, 1682–1684.

McKellop, H.A., D'Lima, D., 2008. How have wear testing and joint simulator studies helped to discriminate among materials

and designs? Journal of the American Academy of Orthopaedic Surgeons 16 (Suppl. 1), S111–S119.
Nevelos, J.E., Ingham, E., Doyle, C., Nevelos, A.B., Fisher, J., 2001. Wear of HIPed and non-HIPed alumina–alumina hip joints under standard and severe simulator testing conditions. Biomaterials 22 (16), 2191–2197.
Pezzotti, G., Porporati, A.A., 2004. Raman spectroscopic analysis of phase-transformation and stress patterns in zirconia hip joints. Journal of Biomedical Optics 9, 372–384.
Pezzotti, G., 2005. Raman piezo-spectroscopic analysis of natural and synthetic biomaterials. Analytical and Bioanalytical Chemistry 381, 577–590.
Pezzotti, G., Tateiwa, T., Zhu, W., Kumakura, T., Yamada, K., Yamamoto, K., 2006. Fluorescence spectroscopic analysis of surface and subsurface residual stress fields in alumina hip joints. Journal of Biomedical Optics 11 024009-1–09.
Pezzotti, G., 2007. Stress microscopy and confocal Raman imaging of load-bearing surfaces in artificial hip joints. Expert Review of Medical Devices 4, 165–189.
Pezzotti, G., Kumakura, T., Yamada, K., Tateiwa, T., Puppulin, L., Zhu, W., Yamamoto, K., 2007. Confocal Raman spectroscopic analysis of cross-linked ultra-high molecular weight polyethylene for application in artificial hip joints. Journal of Biomedical Optics 12 014011-011.
Pezzotti, G., Yamada, K., Sakakura, S., Pitto, R.P., 2008. Raman spectroscopic analysis of advanced ceramic composite for hip prosthesis. Journal of the American Ceramic Society 91, 1199–1206.
Pezzotti, G., Munisso, M.C., Porporati, A.A., Lessnau, K., 2010. On the role of oxygen vacancies and lattice strain in the tetragonal to monoclinic transformation in alumina/zirconia composites and improved environmental stability. Biomaterials 31, 6901–6908.
Puppulin, L., Takahashi, Y., Pezzotti, G., 2011. Polarized Raman analysis of the molecular rearrangement and residual strain on the surface of retrieved polyethylene tibial plates. Acta Biomaterialia 7 (3), 1150–1159.
Saikko, V., 2005. A 12-station anatomic hip joint simulator. Proceedings of the Institution of Mechanical Engineers—Part H: Journal of Engineering in Medicine 219, 437–448.
Scholes, S.C., Green, S.M., Unsworth, A., 2004. The wear of alumina-on-alumina total hip prostheses. J. Bone Joint Surg. Br. 86-B (Suppl. IV), 403.
Sergo, V., 2004. Room-temperature aging of laminate composites of alumina/3-mol%-yttria-stabilized tetragonal zirconia polycrystals. Journal of the American Ceramic Society 87, 247–253.
Singer, I.L., Dvorak, S.D., Wahl, K.J., Scharf, T.W., 2001. Third body processes and friction of solid lubricants studied by *in situ* optical and Raman tribometry. Tribology Series 40, 327–336.
Zhu, W., Puppulin, L., Leto, A., Takahashi, Y., Sugano, N., Pezzotti, G. In situ measurements of local temperature and contact stress area magnitude during wear of ceramic-on-ceramic hip joints. J. Mech. Behavior Biomater., http://dx.doi.org/10.1016/j.jmbbm.2013.01.018, in press.